An Obscured Tidal Disruption Event Manifested as Energetic Mid-infrared Outburst in a Milky-Way-sized Star-forming Galaxy

Hui Liu
University of Science and Technology of China
Ning Jiang (jnac@ustc.edu.cn)
University of Science and Technology of China
Luming Sun
Anhui Normal University
Tinggui Wang
The University of Science and Technology of China https://orcid.org/0000-0002-1517-6792
Roc Cutri
IPAC/Caltech
Xinwen Shu
Anhui Normal University https://orcid.org/0000-0002-7020-4290
Yibo Wang
University of Science and Technology of China
Liming Dou
Guangzhou University
Fabao Zhang
Anhui Normal University
Jiazheng Zhu
University of Science and Technology of China
Zhengfeng Sheng
University of Science and Technology of China

Article

Keywords:

Posted Date: March 15th, 2022

DOI: https://doi.org/10.21203/rs.3.rs-1340699/v1

An Obscured Tidal Disruption Event Manifested as Energetic Mid-infrared Outburst in a Milky-Way-sized Star-forming Galaxy

Hui Liu[1,2,3], Ning Jiang[1,2†], Luming Sun[4], Tinggui Wang[1,2], Roc M. Cutri[5], Xinwen Shu[4], Yibo Wang[1,2], Liming Dou[6], Fabao Zhang[4], Jiazheng Zhu[1,2], Zhenfeng Sheng[1,2]

[1]*CAS Key Laboratory for Research in Galaxies and Cosmology, Department of Astronomy, University of Science and Technology of China, Hefei, Anhui 230026, China*

[2]*School of Astronomy and Space Science, University of Science and Technology of China, Hefei 230026, China*

[3]*Anton Pannekoek Institute for Astronomy (API), University of Amsterdam, Science Park 904, 1098 XH, the Netherlands*

[4]*Department of Physics, Anhui Normal University, Wuhu, Anhui, 241002, China*

[5]*IPAC/Caltech, 1200 E. California Boulevard, Pasadena, CA 91125, USA*

[6]*Department of Astronomy, Guangzhou University, Guangzhou 510006, China*

Stellar tidal disruption events (TDEs) by supermassive black holes[1–3] are now discovered at a rate of about a dozen annually from optical time-domain surveys[4–6]. However, they are puzzlingly overrepresented in post-starburst galaxies[7–9] but almost absent in normal star-forming galaxies. We report an energetic mid-infrared nuclear outburst in a nearby Milky Way-sized star-forming galaxy SDSSJ0103+1401, which did not show any signatures of active galactic nucleus prior to the outburst. The infrared outburst can be perfectly fitted by a dust echo model of an optical-UV transient on time scale of half a year[10–12] with its total radiant energy in the infrared exceeding known supernova. Along with many other analogs[13], we suggest that there exists a new population of dust obscured TDEs in star-forming galaxies, represented by SDSSJ0103+1401, missed by previous optical or soft X-ray surveys, but can be efficiently uncovered by their infrared echoes. The puzzle of post-starburst preference could be highly alleviated with the obscured population taken into consideration.

SDSSJ010320.39+140152.5 (hereafter SDSSJ0103+1401) is known as a spiral galaxy at $z = 0.04181$ with stellar mass similar to the Milky Way (see Methods). It showed an outstanding flare in the mid-infrared (MIR) band starting from 2017, and was selected into our sample of MIR outbursts in nearby galaxies (MIRONG)[13;14], utilizing the multi-epoch photometry of the Wide-field Infrared Survey Explorer (WISE)[15] and its successor Near-Earth Object WISE Reactivation

†jnac@ustc.edu.cn

mission (NEOWISE)[16;17]. The MIR light curves at 3.4 μm (W1) and 4.6 μm (W2) suggest that the galaxy was quiescent before a rising trend starting from 27 Dec 2016 (MJD = 57749, see Figure 1). The luminosity rapidly increased to peak ($L_{4.6\mu\mathrm{m}} = \nu F_\nu(4.6\mu\mathrm{m}) \approx (3.7\pm0.08)\times10^{43}$ erg s^{-1}) and stayed at the high state till 21 Dec 2018 (MJD = 58473), when it began to decline continuously. Interestingly, the galaxy remains invariable in the optical band during the whole outburst. The location of the outburst agrees nicely with the galaxy nucleus ($<$ 0."12 or $<$ 100 pc, see Extended Data Figure 1) within the position uncertainty of the image.

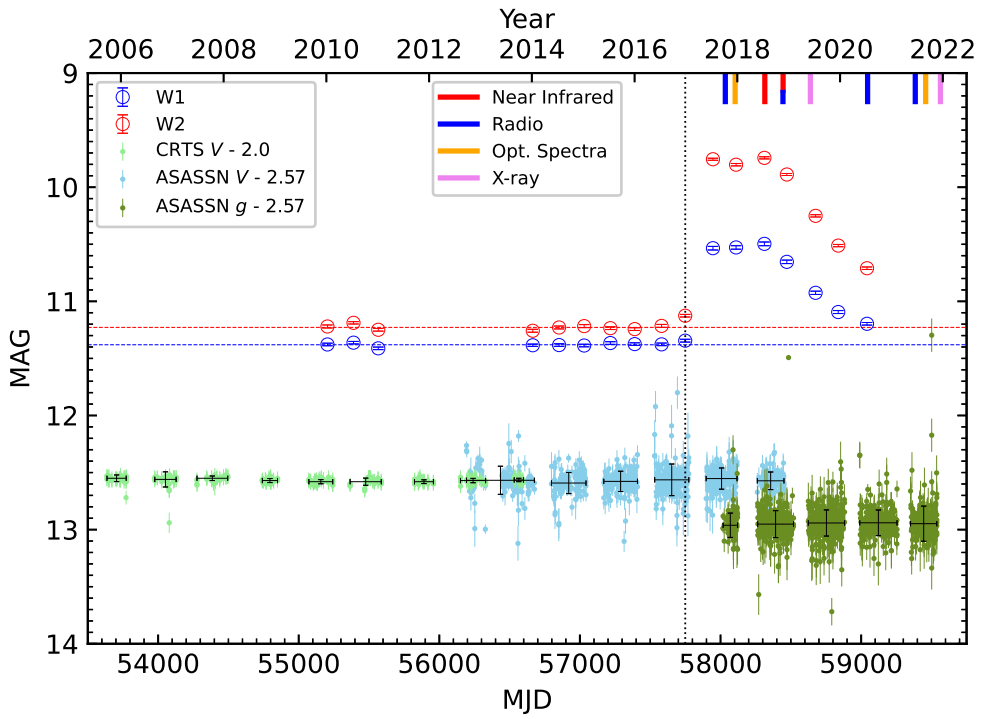

Figure 1: **Multi-wavelength light curves of SDSSJ0103+1401.** We have shown W1 (3.4 μm) and W2 (4.6 μm) light curves with blue and red circles and dashed lines mark their quiescent states. The optical photometry from CRTS (V band) and ASAS-SN survey (V and g bands) are plotted in green, cyan and dark green, respetively, which have been shifted vertically for clarity. Crosses overlaid on optical data points show the magnitude uncertainties at specific time intervals. The vertical dotted line indicates the time when the outburst was initially detected in MIR. Colorful stickers at the top right of the figure label the time when follow-up observations are triggered.

There is no evidence of active galactic nucleus (AGN) in SDSSJ0103+1401 before the outburst. First, it was neither detected by ROSAT all sky X-ray survey[18] nor reported as a radio source indicative of AGN. The optical spectrum from Sloan Digital Sky Survey (SDSS) centered

on the galactic nucleus shows neither broad emission lines nor AGN-like narrow line ratios in the Baldwin-Phillips-Terlevich (BPT) diagnostic diagram[19] (see Extended Data Figure 2). The scenario of obscured AGN can be further excluded by its blue MIR color (W1-W2 = 0.18 ± 0.03)[20;21] and from broad-band spectral energy distribution (SED) fitting (see Extended Data Figure 3), which does not demand an AGN component. The pre-existing optical emission lines and IR emission can be appropriately interpreted by star formation with a rate (SFR) of $\sim 6\ \mathrm{M}_\odot\ \mathrm{yr}^{-1}$ (see Methods).

Multi-wavelength follow-up observations were instantly triggered to explore the unprecedented MIR outburst in SDSSJ0103+1401. The optical spectrum positioned on the galactic nucleus obtained on 16 Dec 2017 shows no significant change with respect to its SDSS spectrum. The NIR images taken by Wide-field InfraRed Camera (WIRCam) at Canada-France-Hawaii Telescope (CFHT) on 16 Jul and 22 Nov in 2018 have also yielded an obvious brightening in H and $\mathrm{K_s}(\mathrm{K})$ bands. Thanks to a much higher spatial resolution of NIR image, the outburst was constrained to within 0."038 (i.e. < 32 pc) to the galaxy center (see Extended Data Figure 1).

The outbursts in the galactic nuclei of quiescent galaxies can usually be attributed to supernova (SNe) or tidal disruption events (TDEs). In either cases, the emitted UV radiation could be absorbed by surrounding dust and reprocessed into infrared[11;12;22–24]. The red infrared color (W1-W2 = 0.7) of SDSSJ0103+1401 at peak indicates strong dust emission. To characterize quantitatively the outburst, we assumed a black-body scenario and calculated its parameters (i.e. dust temperature and size; see Methods) using host-galaxy-light subtracted infrared fluxes in W1 and W2. The dust temperature ranges from 700 to 1000 K. The peak black-body luminosity is $(5.43 \pm 0.20) \times 10^{43}$ erg s^{-1}. A more comprehensive fit to the SED from NIR to MIR yielded similar results (see Extended Data Figure 4 and 5). The integrated observed energy radiated in the IR as of 14 July, 2020 is $E_{\rm tot} = (4.0 \pm 0.1) \times 10^{51}$ erg. If assuming a gray-body spectrum, the inferred radiant energy is $E_{\rm tot} = (3 \sim 9) \times 10^{51}$ erg depending on the grain size and species (e.g., graphite or silicate). The infrared energy is unprecedented for SNe reported so far. Although the most energetic super-luminous SNe have comparable total radiant energy, such as SN 2016aps ($\sim 5 \times 10^{51}$ erg), only a small fraction of their energy is emitted in infrared. In addition, J0103+1401 does not resemble SLSN host galaxies, which typically have masses of less than $10^{9.5}\ \mathrm{M}_\odot$[25] and low metallicities[26]. Considering these and the coincidence between the outburst's location and the galaxy nucleus, we favor a TDE interpretation.

The TDE radiation could be absorbed by dust in the vicinity of supermassive black holes

(SMBHs) and reprocessed into IR band like an echo[10–12]. The so-called IR echo will be apparently luminous in local dusty environments, i.e., encircled by AGN dusty tori[27–29]. Extremely, TDEs could be fully enshrouded by dust and thus completely invisible in the soft X-ray to optical bands. Those obscured candidate events have not been unveiled until very recently by their notable IR echoes[30–33]. It is nevertheless necessary to note that they are all reported in AGNs, and thus the probability of peculiar AGN variability can not be securely ruled out. The emergence of diverse AGN outbursts[34–36] makes the nature of a specific event rather elusive even if TDE scenario is possible.

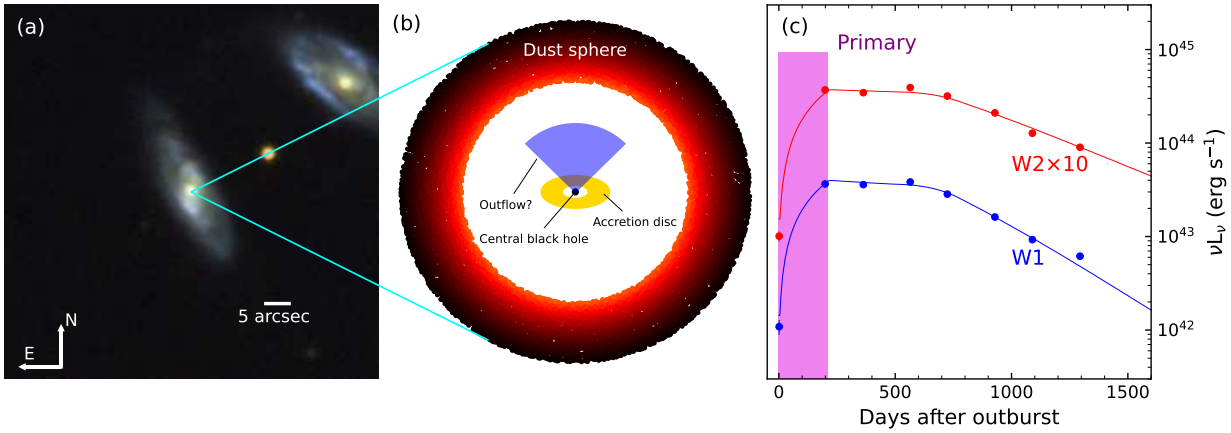

Figure 2: **Host galaxy, schematics and model fitting of the central outburst in SDSSJ0103+1401. a,** The color-composite image of SDSS gri bands with a size of $1.'34 \times 1.'34$. **b,** Schematic structure of the central primary outburst, which is encircled by a dust sphere. The yellow ring is a temporal disk formed by stellar debris after a star disrupted by SMBH. The blue sector represents the outflowing materials giving rise to transient radio emission due to interactions with surrounding gas and dust. **c,** The fitting to light curves in W1 (blue) and W2 (red) bands with dust echo model of TDE. Host-subtracted fluxes are showed as filled circles while solid lines show the best fitting light curves. The fluxes in W2 have been multiplied by 10 for clarity. The violet region denotes the duration and luminosity of the primary outburst.

We try to reproduce the MIR light curve with a straw dust-reprocessing model (see Methods and Figure 2). For simplicity, we consider a thick spherically distributed dust shell, a central UV flare with a constant luminosity illuminates the dust shell for a time of $t_{\rm TDE}$ before it is shutdown. This simple model can fairly well reproduce simultaneously the observed light-curves in W1 and W2. The best fitting model yields a flare with a peak luminosity of $\sim 10^{45}$ erg s^{-1} that occurred around on MJD 57745 (22 Sept 2016) few days before the first detection in MIR and lasted for about 200 days. The integrated energy of the outburst is $(1 \sim 2) \times 10^{52}$ erg, which locates at

the high end of energy distribution of known optically selected TDEs[37], and comparable to Arp 299-B AT1[30], a dust-enshrouded TDE. The dust-echo model shows that the total radiant energy of primary in UV/optical is a factor of a few larger than black-body energy reprocessed in NIR and W1/W2, indicating that significant amount of energy is reprocessed at longer wavelength. The James Webb Space Telescope (JWST)[38] working at a wide wavelength range from 0.6 to 29 μm could provide a powerful way to explore the complete SED of analogs of SDSSJ0103+1401 in infrared and the dust characteristics.

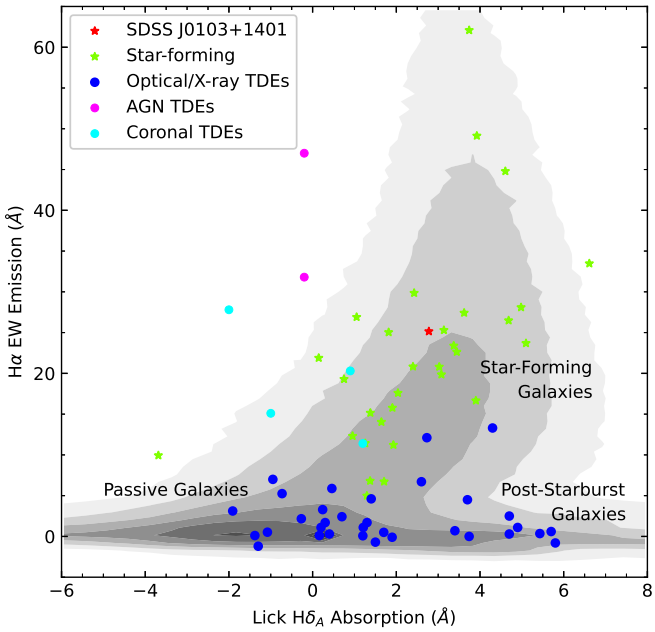

Figure 3: **Spectral indices tracing the recent star formation histories of known TDE hosts and SDSS galaxies[8;39].** We plot Hα EW (sensitive to current star formation) vs. Lick H$\delta_{\rm A}$ absorption (sensitive to star formation over the past Gyr) for each galaxy. We have shown the hosts of known TDE candidates[9;40] selected in optical/X-ray band with filled circles. The hosts of TDEs in AGNs or selected by transient coronal-line emissions are highlighted in fuchsia and cyan. The five-pointed stars represent star-forming galaxies in MIRONG sample[13] with SDSSJ0103+1401 highlighted in red. The overall distribution of SDSS galaxies have been also overplotted with grey contours.

The known obscured TDE candidates are exclusively initially alerted by their IR echoes in either NIR or MIR band because of their severely dimmed emission from X-ray to optical band.

Coincidentally, a remarkable resolved, expanding radio jet has been also uncovered in a nearby system Arp 299B-AT1[30]. Interestingly, our proposed JVLA observation on SDSSJ0103+1401 in 2018 has also yielded out an unresolved (FWHM $\approx$ 3."5) detection at 5.5 GHz. The flux does not show obvious fading as the latest JVLA observation gives a comparable flux at the same band in 2021. Another two epochal observations by VLASS, with resolution of 2."5 at S-band (3 GHz), have also confirmed the compact radio emission in 2017 and 2020, respectively. Given the upper limit SFR of 6 $\mathrm{M_\odot\ yr^{-1}}$ at the center of galaxy, the estimated radio flux upper limit according to the empirical relation[41], ~ 1.6 mJy at 1.4 GHz, is lower than that extrapolated from observed nuclear radio flux (within $\sim$ 2 kpc), ~ 2.5 mJy. Additionally, the high detection rate of radio emission associated with nuclear MIR outburst[42] suggests the compact radio emission could be partially correlated with the MIR flare, which may be checked for variation by future radio observations .

SDSSJ0103+1401 belongs to the main sequence of star-forming galaxies, which differs greatly from the host types of TDEs found in optical or X-ray band (see Figure 3). The post-starburst preference of known TDE hosts is a long-standing puzzle. Scenarios which may lead to the rate enhancement, such as SMBH binaries[43;44], central stellar overdensity[9;45] and velocity anisotropy[46] have been proposed . Those explanations can not address why TDEs are absent in galaxies with current intense star formation[47]. The continued findings of obscured TDEs in ultra luminous infrared galaxies (ULIRGs) indicate promisingly that the overlook by traditional surveys is at least partly due to dust attenuation. Actually, the TDE event rate of starburst ULIRGs is estimated to be even higher than post-starburst galaxies[31]. Aside from ULIRGs which are experiencing violent star formation indicated by their ultra-luminous IR emission, the normal star-forming galaxies lying at the main sequence can also contain large amount of dust in the galactic nucleus that will hide the central SMBHs and activities associated with them.

Our finding indicates strongly that the optical search of TDEs is perhaps seriously biased, which has missed a considerable number of events in dusty environments. This scenario is supported by the very low dust covering factor ($\lesssim 0.01$) of optical TDEs derived from their IR echoes[11;48]. In contrast, the TDEs embedded in more dusty environment can be more efficiently uncovered by their IR echoes. Our systematical IR search has indeed yielded a sample of MIR outbursts (see some examples in Extended Data Figure 9) in star-forming galaxies[13], which bear many similarities with SDSSJ0103+1401. Their corresponding event rate is about 3×10^{-5} $\mathrm{gal^{-1}\ yr^{-1}}$ following the same estimation of the whole sample[13], that is comparable with the observed rate of optical and X-ray TDEs, indicating a significant contribution to the total event rate.

The dust covering factor at sub-pc scale of obscured TDEs in SDSSJ0103+1401 and analogs could be one to two orders of magnitude higher than normal optical TDEs. The huge difference implies that the pc-scale environment has undergone a drastic evolution from the stage of star-forming to post-starburst. The transfer may be triggered by intense feedback from star-formation coupled with possible nuclear activity, which are both regulated by gas supplies. Therefore, further efforts of TDE searching by IR echoes can not only help uncover obscured TDEs, but also enable our deeper understanding of the sub-pc environments of SMBHs in different types of galaxies, which are otherwise extremely challenging to probe.

Methods

Mid-infrared Observation The multi-epoch MIR photometry of SDSSJ0103+1401 are drawn from the Wide-field Infrared Survey Explorer (WISE)[15]. The original WISE survey has mapped the full sky in 4 bands(W1, W2, W3, W4) centered at wavelength of 3.4, 4.6, 12 and 22 μm since Jan 2010 until its hydrogen cryostat was exhausted. The mission has been extended by an additional 4 months as the Near-Earth Object Wide-field Infrared Survey Explorer (NEOWISE)[16] Post-Cryogenic Mission using only W1 and W2 bands. Following a 33-month hibernation period, the WISE instrument recommenced survey operations in Dec 2013, and this post-hibernation mission is referred to as NEOWISE-Reactivation (NEOWISE-R)[17]. The combined WISE and NEOWISE surveys have so far completed approximately 17 visits in W1 and W2 bands with $\sim$ 10-20 exposures per band per visit. The single exposures during a specific visit (typically within one day) can be stacked into one unWISE[49] coadd to improve the signal to noise ratio[50–52]. Since SDSSJ0103+1401 remains invariant before 2017 and thus we tried to adopt the coadded images at those epochs as the reference image of the quiescent state. Then we began to perform the photometry of the outburst stage on the difference images by subtracting the references using HOTPANTS[53]. The fluxes of the outburst were measured with a pointed spread function (PSF). Magnitudes of the galaxy in MIR are summarized in Table 1.

Optical Observations We collected some optical photometry data of SDSSJ0103+1401 from various surveys, including ASAS-SN, CRTS. CRTS is a synoptic astronomical exploration that covers thirty three thousand square degrees of the sky in order to discover rare and interesting transient phenomenon. SDSSJ0103+1401 was observed more than 350 times by CRTS from 2005 to 2016. The CRTS data are aperture-based, unfiltered photometry. ASAS-SN is an automated program to search for new SNe and other astronomical transients. It originally consisted of 2 stations which worked in V band, by the end of 2017, three new stations were added for g band. The ASAS-SN photometric magnitudes are obtained using a two-pixel(16")-radius aperture, and we computed V and g band light curves going back to 3500 days ago from ASAS-SN Sky Patrol. All single exposures of CRTS and ASAS-SN are divided into 16 epochs (9 epochs for CRTS, 7 epochs for ASAS-SN), and median magnitudes are utilised at each epoch. A constant offset -0.57125 is plus to ASAS-SN data to line its V band median magnitude up with CRTS V band median magnitude. All optical photometry data are summarized in Table 2.

Near-Infrared Observations The UKIRT Infrared Deep Sky Survey (UKIDSS) observed SDSSJ0103+1401 in August 2007 in Y, J, H, and K[1] bands. Two new observations in J, H and

[1]J0103+1401 was observed in K band using UKIRT, and in Ks band using CFHT. K and Ks band have slight

Ks bands after the onset of the flare using Wide-field InfraRed Camera (WIRCam) at CFHT on 16 Jul and 22 Nov in 2018 are used to construct infrared SED of the flare. Each observation we exposed twice per band with single exposure time 30, 15, and 11 s, for J, H and Ks bands, respectively. We use SCAMP[54] to re-calibrate WCS of each single exposure based on the catalogues derived by SExtractor[55], and re-sample 2 single frames and combine them into a coadd image using SWarp[56] per band per observation. The flux of SDSSJ0103+1401 in NIR is carried out by PSF photometry using PythonPhot[57] after subtracting UKIDSS images from CFHT images using HOTPANTS[53]. Magnitudes of the flare in NIR are summarized in Table 3.

Spectroscopic Observations SDSSJ0103+1401 was first spectroscopically observed by SDSS on 24 Sept 2000, which shows only strong narrow emission lines. We have taken two new optical spectra with Double Spectrograph (DBSP) mounted on Hale 5m (P200) telescope at Palomar observatory on 16 Dec 2017 immediately after the MIR outburst and on 2 Sept 2021 when the outburst faded down, respectively. The two DBSP observations were configured with slit widths of 1."5 and 2."0, and exposure times of 900 and 1600 s respectively, based on the weather condition. The optical spectra of SDSSJ0103+1401 remained nearly invariant and displayed no conspicuous change over the past two decades (see Extended Data Figure 6). The apparently weaker starlight absorption lines of the first DBSP spectrum in the range 3740-4000 Å could not indicate the emergence of a non-starlight component of outburst since no additional component is required when modelling the DBSP continuum, and it should be due to the bad S/N (only 4.2 pixel^{-1}) in this region. We fitted the SDSS spectrum by *PPXF*, a software implementing the Penalized Pixel-Fitting method to extract the stellar kinematics or populations from absorption-line spectra of galaxies, using a maximum penalized likelihood approach[58]. We then fitted the DBSP spectra with the same stellar populations as the SDSS spectrum. The fitting results show that no additional component is required (e.g., a reddened power-law continuum from AGN).

Multi-Gaussian fitting applied to the Hα region of DBSP spectra yields no evident broad component, that is consistent with the SDSS spectrum. The narrow emission line ratios of all spectra put the galaxy in the star-forming region in the BPT diagram (see Extended Data Figure 2). In brief, the optical spectra, agreeing with the photometry, is also not aware of the MIR outburst and it does not show any signature of AGN before and after.

X-ray Observations J0103+1401 was observed by Swift/XRT on 5 Jun 2019 with a net exposure of 1.666 ks and 16 Dec 2021 with a net exposure of 4.031 ks. We reprocessed the event file with the task "xrtpipeline" and selected the event file which operated in Photon Counting mode.

difference with their effective wavelength $\sim$ 2.20 and 2.13 μm respectively. Here we ignored the small difference.

No significant detection ($\lesssim 1\sigma$) is found in both epochs. We stacked their photon events together and extracted only 5 photons from a circle with radius 36" (two times of resolution) region at the source position. The background is extracted from a source-free annulus region with inner radius of 40 pixel and outer radius of 60 pixel. 3σ upper limit of the net count rate in 0.3-10 keV band is 1.7×10^{-3} s^{-1} derived from the stacked image. If assuming a Galactic absorbed powerlaw with a fixed photon index of $\Gamma = 2$ ($N_H^G = 3.55 \times 10^{20}$ cm^{-2} [59]), the unabsorbed 3σ upper limit flux at 0.3-10 keV band is then estimated to be 6×10^{-14} erg cm^{-2} s^{-1} using the tool of "PIMMS", that is 2.3×10^{41} erg s^{-1}.

Radio Observations SDSSJ0103+1401 was observed at C-band (central frequency of 5.5 GHz) with the VLA in its moderately compact C configuration on 21 Nov 2018 (program code, 18B-086) and 20 Jun 2021 (program code, 21A-146), respectively. The data were reduced following standard procedures with the CASA package. For both epoch observations, flux density calibration was conducted using 3C48, whereas the nearby source J0112+2244 was used to determine the complex gain solutions which were interpolated to SDSSJ0103+1401. After removing the RFI, the data were imaged using the CLEAN algorithm, with Briggs weighting and ROBUST parameter of 0. The final cleaned map suggests a deconvolved source size of 2."0×1."4 for epoch I and 2."2×1."4 for epoch II observation. SDSSJ0103+1401 is clearly detected as a compact source, with an integrated flux density of 1.34 ± 0.05 and 1.25 ± 0.03 mJy, respectively, which were measured using the CASA task IMFIT. Besides that, the Very Large Array Sky Survey (VLASS) has another two epochal observations at 3 GHz (S-band) on 8 Oct 2017 and 16 Jul 2020. They are also unresolved at resolution of 2."5, giving an integrated flux of 1.61 ± 0.10 and 1.90 ± 0.26 mJy, respectively.

Unfortunately, no reliable radio maps on this field exist before the outburst, which can be used to check the variability and indicate whether the compact radio emission is associated with the outburst. It is worth mentioning that SDSSJ0103+1401 was observed by NVSS [60] survey. However, due to poor spatial resolution (45"), we cannot reliably deblend it from its companion galaxy SDSSJ010318.13+140215.6 (see left panel of Figure 2), which can also be seen in VLASS images with higher radio flux.

SED of Host Galaxy We modeled the multi-wavelength SED of SDSSJ0103+1401 with Code Investigating GALaxy Emission (CIGALE [61]), which builds a galaxy SED modeling with stellar, dust and AGN components. In our fitting, we used a delayed star formation history (SFH) assuming a single starburst with an exponential decay. We employed single stellar population(SSP) of Bruzual [62] and took into account the dust attenuation module based on modified Calzetti [63] law.

The default nebular emission model[64] was added in our fitting. For dust emission, we utilized a model provided by Dale[65]. AGN emission was calculated by the AGN model of Fritz[66]. Extended Data Figure 3 shows the SED fitting of photometry spanning 16 bands (FUV, NUV, u, g, r, i, z, y, Y, J, H, K, W1, W2, W3, W4). All photometric fluxes have been corrected for Galactic extinction[59;67]. Being well fitted by stellar and dust emission, the SED does not demand AGN component at all, further corroborating an inactive SMBH with the obscured AGN scenario also ruled out. Moreover, the best fitting shows the host galaxy of SDSSJ0103+1401 has a high SFR of $\sim 6\,\mathrm{M_\odot\,yr^{-1}}$ with total stellar mass of $\sim 10^{10.5}\,\mathrm{M_\odot}$. We summarised Galactic extinction-corrected fluxes and some important fitting parameters in Table 4.

Black hole mass The $M_{\rm BH}$ of inactive galaxies are generally estimated by empirical relations between $M_{\rm BH}$ and their host galaxies, i.e., stellar velocity dispersion ($\sigma_\star$) or bulge mass ($M_{\rm bulge}$), albeit with large uncertainties (0.3-0.4 dex) for individual source[68]. We adopt the formulas given by two widely-used literature[68;69]. Detailedly, the $M_{\rm BH}$ predicted by $M_{\rm BH}$-$\sigma_\star$ relation yields 1.15×10^7 and $2.95\times10^6\,\mathrm{M_\odot}$, respectively, provided a $\sigma_\star$ value of 94.2 km s^{-1} as measured from its SDSS spectrum. On the other hand, the bulge-disk structural decomposition[70] gives a r-band bulge-to-total flux ratio of 0.14, suggesting a $M_{\rm bulge}$ of $4.7\times10^9\,\mathrm{M_\odot}$ and thus a $M_{\rm BH}$ of 1.17×10^7 and $1.38\times10^7\,\mathrm{M_\odot}$ if naively assuming a classical bulge.

Location of the MIR outburst The host of SDSSJ0103+1401 is a star-forming galaxy and thus the probability of SNe origin is not negligible. However, SNe are usually off-centered and more likely found in the spiral arms of galaxies[71]. Aiming at checking its physical location, we have carefully measured the center of the outburst in W2 difference images (with amplitude variability larger than W1 band) by fitting a 2-dimension Gaussian function. The offset of the outburst to the galaxy center is constrained to be $\sim 0.12\pm0.08$ arc (see Extended Data Figure 1). As we have detected obvious NIR variability between CFHT and UKIDSS observations, which possess higher spatial resolutions than WISE images, we then tried to obtain more precise measurement of the outburst location with aid of them. Before image subtraction, we first aligned the two images with software Scamp[54] by registering the stars in the field, with the caveat that the proper motions of stars (given by Gaia Data Release 2[72]) between the two observations are non-negligible and need to be corrected. The result shows that the outburst is still exactly located at galaxy center with an offset $\sim 0.038\pm0.040$ arc, that is 32 ± 34 pc. The location of the outburst is in disfavor with SNe scenario but indicates a likely origin associated with the central SMBH.

IR SED With robust variability detected in MIR and NIR bands, we tried to fit the quasi-simultaneous IR SED under dust emission scheme. Since only two epochs of NIR observations

are available, we chose to infer the MIR photometry at similar time with NIR epochs using linear interpolation. The SED can be nicely fitted by pure blackbody model (see Extended Data Figure 5) with reduced χ^2 = 3.4 and 2.7 for both epochs, respectively. Assuming an isotropic dust emission, their luminosity are correspondingly $L_{\rm IR} = (5.36 \pm 0.43) \times 10^{43}$ erg s^{-1}(first epoch) and $(4.44 \pm 0.45) \times 10^{43}$ erg s^{-1}(second epoch). Since blackbody model is acceptable to describe the IR emission, we then derived the blackbody luminosity in other epochs and integrated them over time. The total emitted energy as of Jul 2020 is $E_{\rm tot} = (4.0 \pm 0.1) \times 10^{51}$ erg. As the real dust emission might be not perfect blackbody, we have also tried to perform modeling by taking the dust absorption efficiency into consideration[13] and the obtained dust luminosity is comparable with blackbody model. The integrated energy of SDSSJ0103+1401 is even higher than superluminous SNe (SLSNe[73–76]) and comparable with the extremely energetic source SN2016aps[77], which has radiated $\gtrsim 5 \times 10^{51}$ erg. If it is a SN producing the MIR outburst in SDSSJ0103+1401, it would be one of the most energetic SNe to date. Moreover, none SNe show such strong emission in the MIR to our knowledge. All of these characteristics suggest an unlikely SN scenario.

Dust Echo Model Assuming that the IR emission is originated from dust echo of an obscured TDE, we tried to explore the properties of its primary UV-optical radiation by fitting the observed MIR light curves with a parametric dust echo model[10;33]. The model assumes that the TDE UV-optical radiation starts from time $\rm t_0$, lasts for a duration $t_{\rm TDE}$, and has a luminosity L_0. The surrounding dust is distributed uniformly in a spherical layer between inner radius $r_{\rm in}$ and outer radius $r_{\rm out}$. The dust is a 1:1 mixture of graphite and silicate. All dust grains have the same initial radius a_0 with a number density $n_{\rm d}$ independent of radius. Under above assumptions, we calculated the heating of dust by radiations, the dust sublimation, the IR re-radiation from dust, and the observed multi-band light curves. The model has seven free parameters. Three are related to the UV-optical radiation of the TDE: L_0, t_0, and $E_{\rm tot}$ (calculated as $L_0 t_{\rm TDE}$) and the other four are related to the dust: $r_{\rm in}$, $r_{\rm out}$, a_0, and $n_{\rm d}$. We modeled the MIR light curves using a Markov Chain Monte Carlo (MCMC) approach, assuming that all the parameters have log-uniform prior probability distributions. The posterior probability density distributions obtained from the MCMC approach are shown in Extended Data Figure 8. Note that we do not show the distribution of $r_{\rm in}$, because it is not well bounded and only an upper limit can be obtained. We also list the confidence interval of the parameters with 99.7% probability in Table 5. The model yielding the minimum chi-square is shown in Figure 2. The dust echo model matches the observed IR light curves with only $< 10\%$ discrepancy for most data points, and the discrepancy may be caused by the simplicity of our model assumption (e.g. geometry of the dust distribution and types of the dust grain).

Data availability The observational data from WISE and NEOWISE surveys are available through NASA/IPAC Infrared Science Archive (IRSA). The unWISE coadds data can be downloaded from (https://portal.nersc.gov/project/cosmo/temp/ameisner/neo6/). The optical photometry from ASASSN and CRTS are available from their corresponding websites (https://asas-sn.osu.edu/ and http://nesssi.cacr.caltech.edu/DataRelease/). UKIDSS NIR data and VLASS radio data are included in WFCAM Science Archive and NRAO Science Data Archive, respectively. The authors can provide other data that support the findings of this study upon request.

Code availability All codes that support the plots within this article are available from the authors upon reasonable request.

References

1. Hills, J. G. Possible power source of Seyfert galaxies and QSOs. Nature **254**, 295–298 (1975).

2. Rees, M. J. Tidal disruption of stars by black holes of 10^6-10^8 solar masses in nearby galaxies. Nature **333**, 523–528 (1988).

3. Phinney, E. S. Manifestations of a Massive Black Hole in the Galactic Center. In Morris, M. (ed.) The Center of the Galaxy, vol. 136, 543 (1989).

4. van Velzen, S., Holoien, T. W. S., Onori, F., Hung, T. & Arcavi, I. Optical-Ultraviolet Tidal Disruption Events. Space Science Reviews **216**, 124 (2020).

5. van Velzen, S. et al. Seventeen Tidal Disruption Events from the First Half of ZTF Survey Observations: Entering a New Era of Population Studies. Astrophys. J. **908**, 4 (2021).

6. Gezari, S. Tidal Disruption Events. Ann. Rev. Astron. Astrophys. **59** (2021).

7. Arcavi, I. et al. A Continuum of H- to He-rich Tidal Disruption Candidates With a Preference for E+A Galaxies. Astrophys. J. **793**, 38 (2014).

8. French, K. D., Arcavi, I. & Zabludoff, A. Tidal Disruption Events Prefer Unusual Host Galaxies. Astrophys. J. **818**, L21 (2016).

9. French, K. D., Wevers, T., Law-Smith, J., Graur, O. & Zabludoff, A. I. The Host Galaxies of Tidal Disruption Events. Space Science Reviews **216**, 32 (2020).

10. Lu, W., Kumar, P. & Evans, N. J. Infrared emission from tidal disruption events - probing the pc-scale dust content around galactic nuclei. Mon. Not. R. Astron. Soc. **458**, 575–581 (2016).

11. van Velzen, S., Mendez, A. J., Krolik, J. H. & Gorjian, V. Discovery of Transient Infrared Emission from Dust Heated by Stellar Tidal Disruption Flares. Astrophys. J. **829**, 19 (2016).

12. Jiang, N. et al. The WISE Detection of an Infrared Echo in Tidal Disruption Event ASASSN-14li. Astrophys. J. **828**, L14 (2016).

13. Jiang, N. et al. Mid-infrared Outbursts in Nearby Galaxies (MIRONG). I. Sample Selection and Characterization. Astrophys. J. **252**, 32 (2021).

14. Wang, Y. et al. Mid-infrared Outbursts in Nearby Galaxies (MIRONG). II. Optical Spectroscopic Follow-up. Astrophys. J. **258**, 21 (2022).

15. Wright, E. L. et al. The Wide-field Infrared Survey Explorer (WISE): Mission Description and Initial On-orbit Performance. Astron. J. **140**, 1868–1881 (2010).

16. Mainzer, A. et al. Preliminary Results from NEOWISE: An Enhancement to the Wide-field Infrared Survey Explorer for Solar System Science. Astrophys. J. **731**, 53 (2011).

17. Mainzer, A. et al. Initial Performance of the NEOWISE Reactivation Mission. Astrophys. J. **792**, 30 (2014).

18. Truemper, J. ROSAT-A New Look at the X-ray Sky. Science **260**, 1769–1771 (1993).

19. Baldwin, J. A., Phillips, M. M. & Terlevich, R. Classification parameters for the emission-line spectra of extragalactic objects. **93**, 5–19 (1981).

20. Stern, D. et al. Mid-infrared Selection of Active Galactic Nuclei with the Wide-Field Infrared Survey Explorer. I. Characterizing WISE-selected Active Galactic Nuclei in COSMOS. Astrophys. J. **753**, 30 (2012).

21. Yan, L. et al. Characterizing the Mid-infrared Extragalactic Sky with WISE and SDSS. Astron. J. **145**, 55 (2013).

22. Dwek, E. The infrared echo of a type II supernova with a circumstellar dust shell : applications to SN 1979c and SN 1980k. Astrophys. J. **274**, 175–183 (1983).

23. Graham, J. R. et al. Discovery of an IR echo from a supernova dust cloud. Nature **304**, 709–710 (1983).

24. Miller, A. A. et al. New Observations of the Very Luminous Supernova 2006gy: Evidence for Echoes. Astron. J. **139**, 2218–2229 (2010).

25. Frohmaier, C. et al. From core collapse to superluminous: the rates of massive stellar explosions from the Palomar Transient Factory. Mon. Not. R. Astron. Soc. **500**, 5142–5158 (2021).

26. Perley, D. A. et al. Host-galaxy Properties of 32 Low-redshift Superluminous Supernovae from the Palomar Transient Factory. Astrophys. J. **830**, 13 (2016).

27. Dou, L. et al. Discovery of a Mid-infrared Echo from the TDE Candidate in the Nucleus of ULIRG F01004-2237. Astrophys. J. **841**, L8 (2017).

28. Jiang, N. et al. Mid-infrared Flare of TDE Candidate PS16dtm: Dust Echo and Implications for the Spectral Evolution. Astrophys. J. **850**, 63 (2017).

29. Jiang, N. et al. Infrared Echo and Late-stage Rebrightening of Nuclear Transient Ps1-10adi: Exploring the Torus with Tidal Disruption Events in Active Galactic Nuclei. Astrophys. J. **871**, 15 (2019).

30. Mattila, S. et al. A dust-enshrouded tidal disruption event with a resolved radio jet in a galaxy merger. Science **361**, 482–485 (2018).

31. Kool, E. C. et al. AT 2017gbl: a dust obscured TDE candidate in a luminous infrared galaxy. Mon. Not. R. Astron. Soc. **498**, 2167–2195 (2020).

32. Yang, Q. et al. An Unusual Mid-infrared Flare in a Type 2 AGN: An Obscured Turning-on AGN or Tidal Disruption Event? Astrophys. J. **885**, 110 (2019).

33. Sun, L. et al. A Mid-infrared Flare in the Active Galaxy MCG-02-04-026: Dust Echo of a Nuclear Transient Event. Astrophys. J. **898**, 129 (2020).

34. Kankare, E. et al. A population of highly energetic transient events in the centres of active galaxies. Nature Astronomy **1**, 865–871 (2017).

35. Trakhtenbrot, B. et al. A new class of flares from accreting supermassive black holes. Nature Astronomy **3**, 242–250 (2019).

36. Malyali, A. et al. AT 2019avd: a novel addition to the diverse population of nuclear transients. Astron. Astrophys. **647**, A9 (2021).

37. Lu, W. & Kumar, P. On the Missing Energy Puzzle of Tidal Disruption Events. Astrophys. J. **865**, 128 (2018).

38. Gardner, J. P. et al. The James Webb Space Telescope. Space Science Reviews **123**, 485–606 (2006).

39. Graur, O. et al. A Dependence of the Tidal Disruption Event Rate on Global Stellar Surface Mass Density and Stellar Velocity Dispersion. Astrophys. J. **853**, 39 (2018).

40. Sazonov, S. et al. First tidal disruption events discovered by SRG/eROSITA: X-ray/optical properties and X-ray luminosity function at z < 0.6. Mon. Not. R. Astron. Soc. **508**, 3820–3847 (2021).

41. Davies, L. J. M. et al. Galaxy And Mass Assembly: the 1.4 GHz SFR indicator, SFR-M_* relation and predictions for ASKAP-GAMA. Mon. Not. R. Astron. Soc. **466**, 2312–2324 (2017).

42. Dai, B. B. et al. Compact Radio Emission from Nearby Galaxies with Mid-infrared Nuclear Outbursts. Astrophys. J. **896**, L27 (2020).

43. Chen, X., Madau, P., Sesana, A. & Liu, F. K. Enhanced Tidal Disruption Rates from Massive Black Hole Binaries. Astrophys. J. **697**, L149–L152 (2009).

44. Coughlin, E. R., Armitage, P. J., Lodato, G. & Nixon, C. J. The Influence of Black Hole Binarity on Tidal Disruption Events. Space Science Reviews **215**, 45 (2019).

45. Stone, N. C. & Metzger, B. D. Rates of stellar tidal disruption as probes of the supermassive black hole mass function. Mon. Not. R. Astron. Soc. **455**, 859–883 (2016).

46. Stone, N. C., Generozov, A., Vasiliev, E. & Metzger, B. D. The delay time distribution of tidal disruption flares. Mon. Not. R. Astron. Soc. **480**, 5060–5077 (2018).

47. Guillochon, J. Black holes: Crime in search of a crime scene. Nature Astronomy **1**, 0068 (2017).

48. Jiang, N. et al. Infrared Echoes of Optical Tidal Disruption Events: $\sim$1% Dust-covering Factor or Less at Subparsec Scale. Astrophys. J. **911**, 31 (2021).

49. Lang, D. unWISE: Unblurred Coadds of the WISE Imaging. Astron. J. **147**, 108 (2014).

50. Meisner, A. M., Lang, D. & Schlegel, D. J. Full-depth Coadds of the WISE and First-year NEOWISE-reactivation Images. Astron. J. **153**, 38 (2017).

51. Meisner, A. M., Lang, D. & Schlegel, D. J. Time-resolved WISE/NEOWISE Coadds. Astron. J. **156**, 69 (2018).

52. Meisner, A. M., Lang, D., Schlafly, E. F. & Schlegel, D. J. unWISE Coadds: The Five-year Data Set. **131**, 124504 (2019).

53. Becker, A. HOTPANTS: High Order Transform of PSF ANd Template Subtraction (2015).

54. Bertin, E. Automatic Astrometric and Photometric Calibration with SCAMP. In Gabriel, C., Arviset, C., Ponz, D. & Enrique, S. (eds.) Astronomical Data Analysis Software and Systems XV, vol. 351 of Astronomical Society of the Pacific Conference Series, 112 (2006).

55. Bertin, E. & Arnouts, S. SExtractor: Software for source extraction. **117**, 393–404 (1996).

56. Bertin, E. et al. The TERAPIX Pipeline, vol. 281 of Astronomical Society of the Pacific Conference Series, 228 (2002).

57. Jones, D. O., Scolnic, D. M. & Rodney, S. A. PythonPhot: Simple DAOPHOT-type photometry in Python (2015).

58. Cappellari, M. & Emsellem, E. Parametric Recovery of Line-of-Sight Velocity Distributions from Absorption-Line Spectra of Galaxies via Penalized Likelihood. **116**, 138–147 (2004).

59. HI4PI Collaboration et al. HI4PI: A full-sky H I survey based on EBHIS and GASS. Astron. Astrophys. **594**, A116 (2016).

60. Condon, J. J. et al. The NRAO VLA Sky Survey. Astron. J. **115**, 1693–1716 (1998).

61. Boquien, M. et al. CIGALE: a python Code Investigating GALaxy Emission. Astron. Astrophys. **622**, A103 (2019).

62. Bruzual, G. & Charlot, S. Stellar population synthesis at the resolution of 2003. Mon. Not. R. Astron. Soc. **344**, 1000–1028 (2003).

63. Calzetti, D. et al. The Dust Content and Opacity of Actively Star-forming Galaxies. Astrophys. J. **533**, 682–695 (2000).

64. Inoue, A. K. Rest-frame ultraviolet-to-optical spectral characteristics of extremely metal-poor and metal-free galaxies. Mon. Not. R. Astron. Soc. **415**, 2920–2931 (2011).

65. Dale, D. A. et al. A Two-parameter Model for the Infrared/Submillimeter/Radio Spectral Energy Distributions of Galaxies and Active Galactic Nuclei. Astrophys. J. **784**, 83 (2014).

66. Fritz, J., Franceschini, A. & Hatziminaoglou, E. Revisiting the infrared spectra of active galactic nuclei with a new torus emission model. Mon. Not. R. Astron. Soc. **366**, 767–786 (2006).

67. Güver, T. & Özel, F. The relation between optical extinction and hydrogen column density in the Galaxy. Mon. Not. R. Astron. Soc. **400**, 2050–2053 (2009).

68. Kormendy, J. & Ho, L. C. Coevolution (Or Not) of Supermassive Black Holes and Host Galaxies. Ann. Rev. Astron. Astrophys. **51**, 511–653 (2013).

69. McConnell, N. J. & Ma, C.-P. Revisiting the Scaling Relations of Black Hole Masses and Host Galaxy Properties. Astrophys. J. **764**, 184 (2013).

70. Simard, L., Mendel, J. T., Patton, D. R., Ellison, S. L. & McConnachie, A. W. A Catalog of Bulge+disk Decompositions and Updated Photometry for 1.12 Million Galaxies in the Sloan Digital Sky Survey. Astrophys. J. **196**, 11 (2011).

71. McMillan, R. J. & Ciardullo, R. Constraining the Ages of Supernova Progenitors. I. Supernovae and Spiral Arms. Astrophys. J. **473**, 707 (1996).

72. Gaia Collaboration et al. Gaia Data Release 2. Observational Hertzsprung-Russell diagrams. Astron. Astrophys. **616**, A10 (2018).

73. Smith, N. et al. SN 2006gy: Discovery of the Most Luminous Supernova Ever Recorded, Powered by the Death of an Extremely Massive Star like η Carinae. Astrophys. J. **666**, 1116–1128 (2007).

74. Drake, A. J. et al. Discovery of the Extremely Energetic Supernova 2008fz. Astrophys. J. **718**, L127–L131 (2010).

75. Chatzopoulos, E. et al. SN 2008am: A Super-luminous Type IIn Supernova. Astrophys. J. **729**, 143 (2011).

76. Benetti, S. et al. The supernova CSS121015:004244+132827: a clue for understanding super-luminous supernovae. Mon. Not. R. Astron. Soc. **441**, 289–303 (2014).

77. Nicholl, M. et al. An extremely energetic supernova from a very massive star in a dense medium. Nature Astronomy **4**, 893–899 (2020).

78. Kewley, L. J., Dopita, M. A., Sutherland, R. S., Heisler, C. A. & Trevena, J. Theoretical Modeling of Starburst Galaxies. Astrophys. J. **556**, 121–140 (2001).

79. Kauffmann, G. et al. The host galaxies of active galactic nuclei. Mon. Not. R. Astron. Soc. **346**, 1055–1077 (2003).

80. Kewley, L. J., Groves, B., Kauffmann, G. & Heckman, T. The host galaxies and classification of active galactic nuclei. Mon. Not. R. Astron. Soc. **372**, 961–976 (2006).

Acknowledgements We acknowledge the financial support by NSFC (11833007, 12073025, 11421303, 12192220, 12192221), the B-type Strategic Priority Program of the Chinese Academy of Sciences (Grant No. XDB41000000), and China Manned Spaced Project (CMS-CSST-2021-B11). This research uses data obtained through the Telescope Access Program (TAP). Observations obtained with the Hale Telescope at Palomar Observatory were obtained as part of an agreement between the National Astronomical Observatories, Chinese Academy of Sciences, and the California Institute of Technology.

Author contributions N.J. designed the project. H.L. reduced and analyzed multi-wavelength light curves, CFHT images and SED fitting. X.S. and F.Z. reduced and analyzed radio data. Y.W. reduced and analyzed the optical spectra. L.D. reduced the Swift X-ray data. R.C. checked the WISE photometry. L.S. fitted the light curves with dust echo model. N.J. and H.L. jointly drafted the manuscript. T.W. provided critical feedback and revised the manuscript significantly. All authors discussed and gave comments on the contents of the paper.

Competing Interests The authors declare that they have no competing financial interests.

Correspondence and request for materials Please contact N.J. at (jnac@ustc.edu.cn).

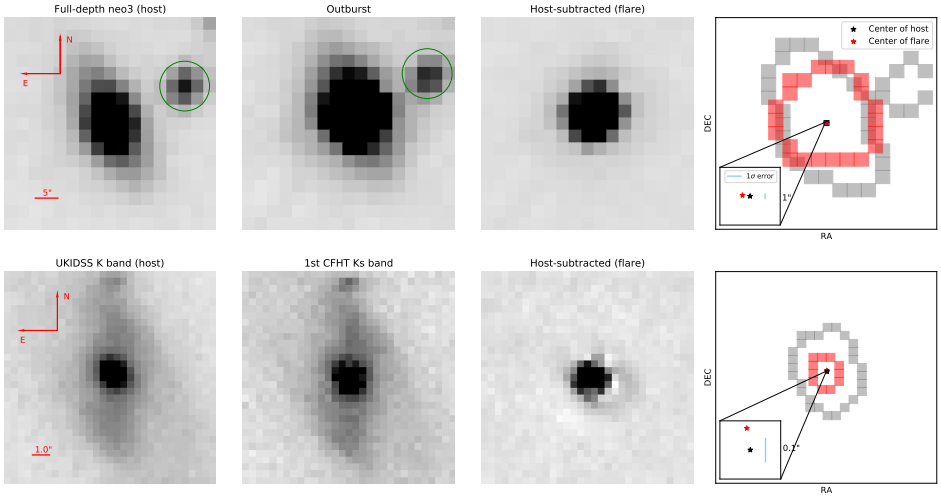

Extended Data Figure 1: **Localisation of the flare from MIR(upper row) and NIR(lower row).** From left to right the columns show the quiescent/outburst state of SDSSJ0103+1401, the host-subtracted flare, and the difference of location between host and flare. The source enclosed by a green circle is a foreground star.

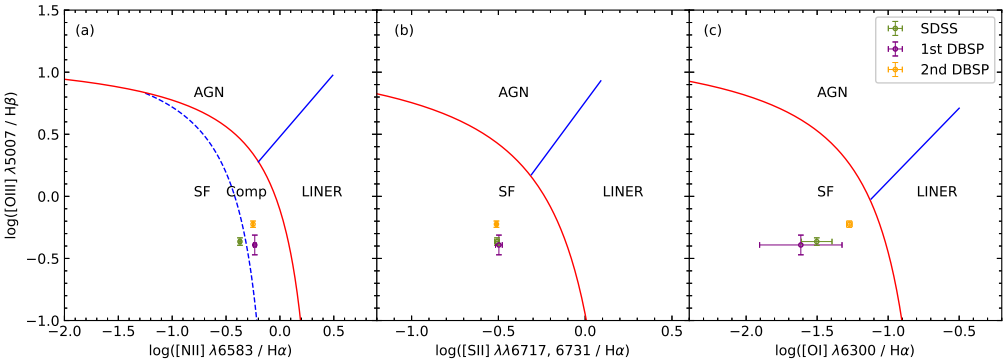

Extended Data Figure 2: **BPT diagrams of SDSSJ0103+1401. a,** The [O III]/Hβ verse [N II]/Hα diagnostic diagram. The Ke01[78] extreme starburst line and the Ka03[79] classification line are shown as the red solid and blue dashed lines, respectively. **b,** The [O III]/Hβ verse [S II]/Hα diagnostic diagram. **c,** The [O III]/Hβ versus [O I]/Hα diagnostic diagram[80]. The emission line ratios reveal SDSSJ0103+1401 is a star-forming galaxy without active galactic nucleus(AGN).

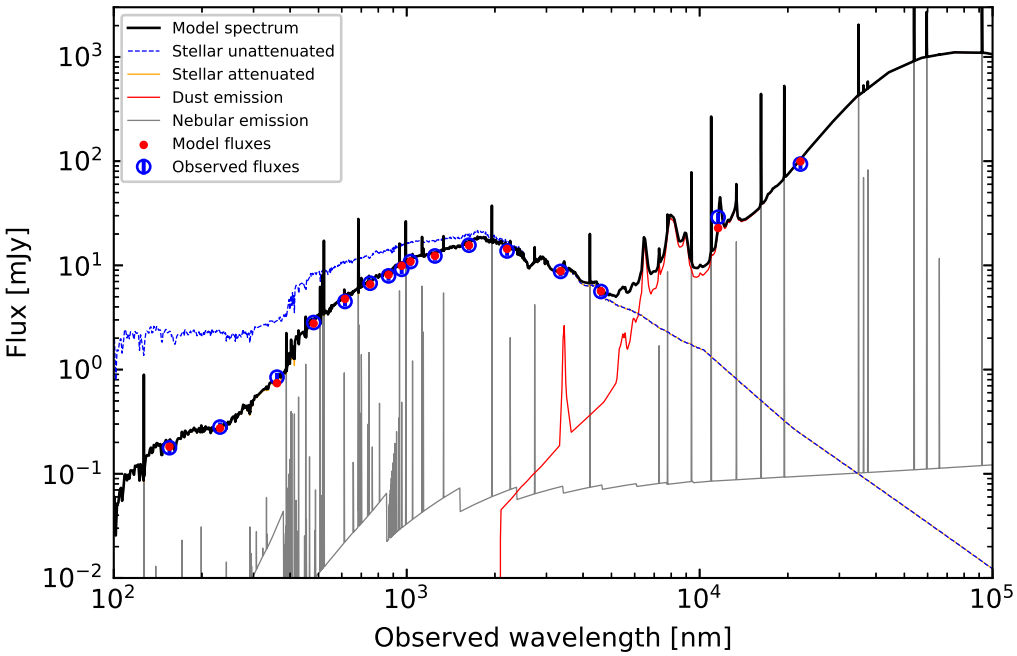

Extended Data Figure 3: **Broad spectral energy distribution (SED) of the host galaxy.** The SED(in flux density per unit frequency), in observer's rest frame, is fitted well using CIGALE with reduced $\chi^2 = 0.51$. The best fitting shows no AGN component at all.

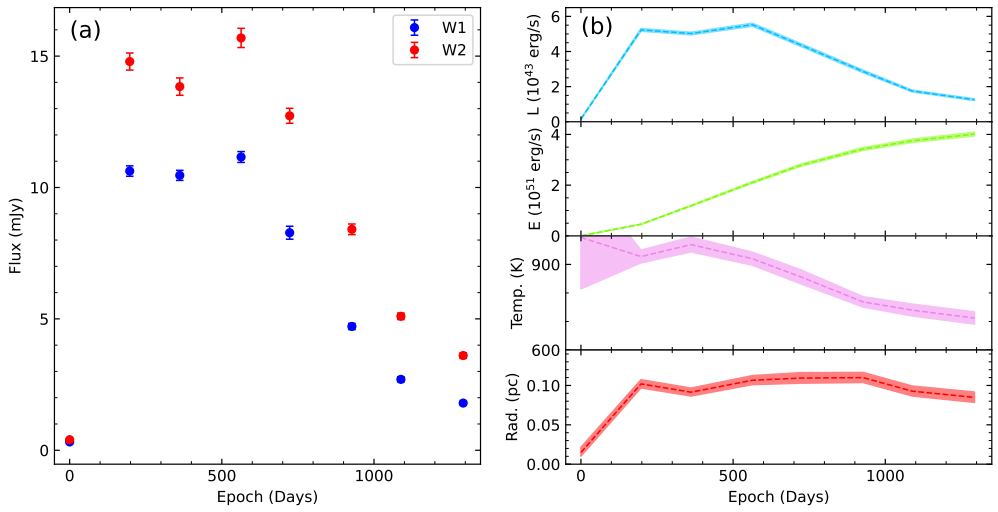

Extended Data Figure 4: **Total radiant energy in infrared of the host-subtracted flare. a,** Flux of the flare after it was first detected in middle infrared. **b,** The lower two panels represent parameters(temperature and size) under the assumption of a blackbody scheme. The upper two panels give the luminosity and cumulative radiant energy in IR.

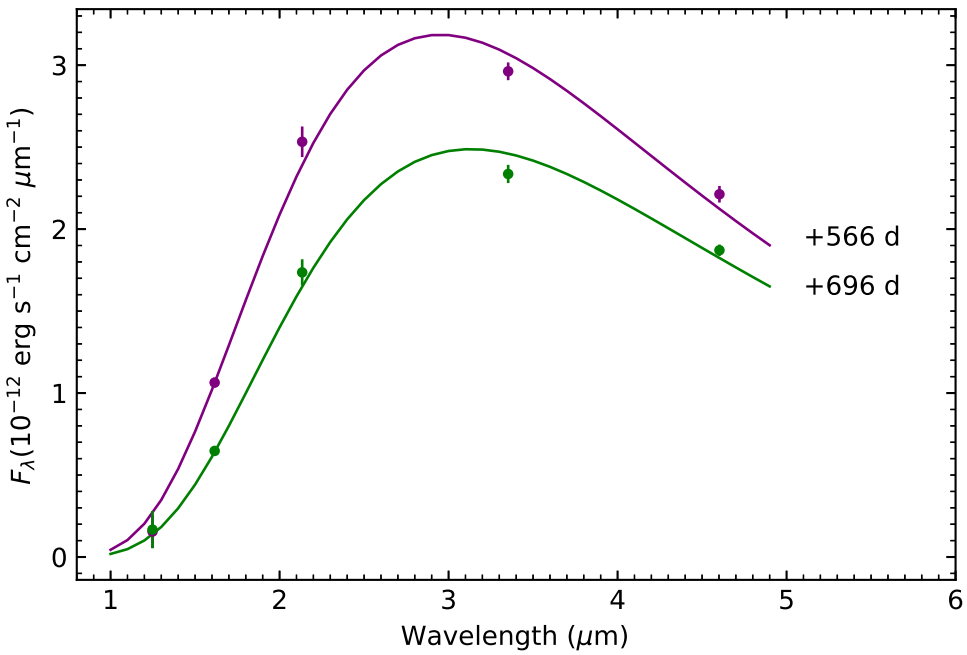

Extended Data Figure 5: **Infrared SED of host-subtracted flare.** The circle dots are observed (or linear-interpolation) fluxes in J, H, Ks and W1, W2 bands, respectively. The lines labelled with phases (days after the first detection in MIR) are the best blackbody fitting curves with χ^2/dof=3.4 (purple) and 2.7 (green).

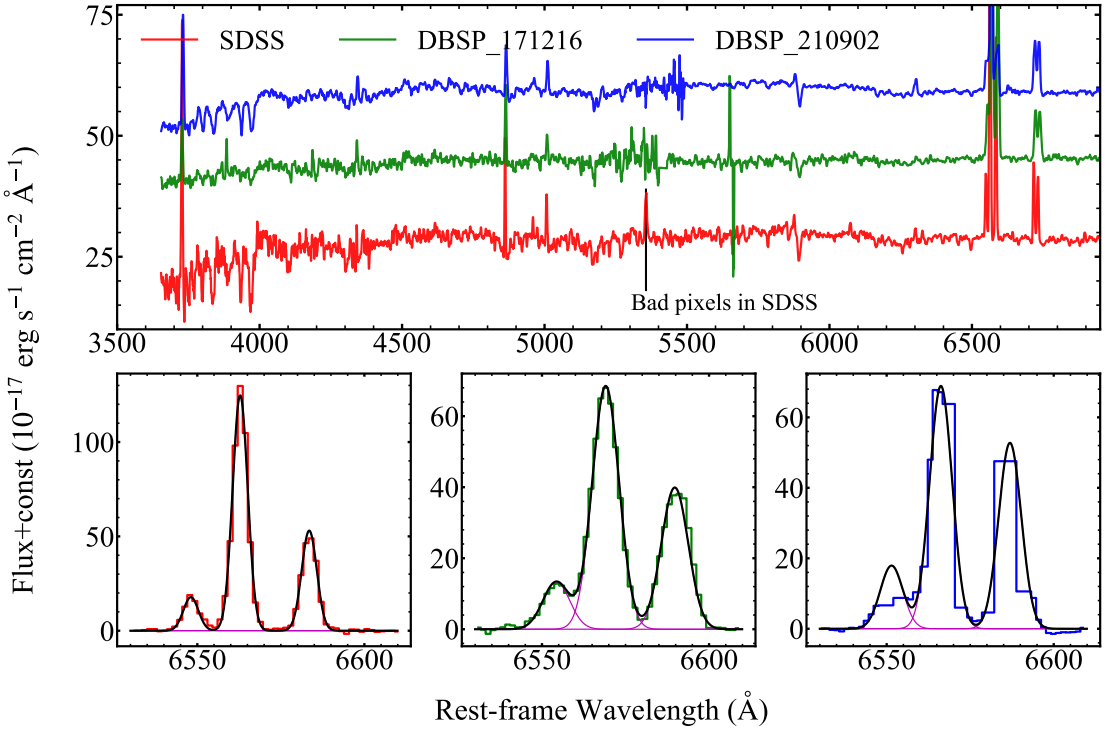

Extended Data Figure 6: **SDSS, DBSP spectra and** Hα **emission lines of SDSSJ0103+1401.** DBSP spectra have been offset for clarity. The lower panels show the zoom-in region of continuum-subtracted Hα emission line, with the black curves representing the best-fit model of multiple narrow components (purple curves). Note that there is a fake line feature in SDSS spectrum (marked by black line on the top panel) due to the bright sky and its residuals based on the SDSS bitmasks.

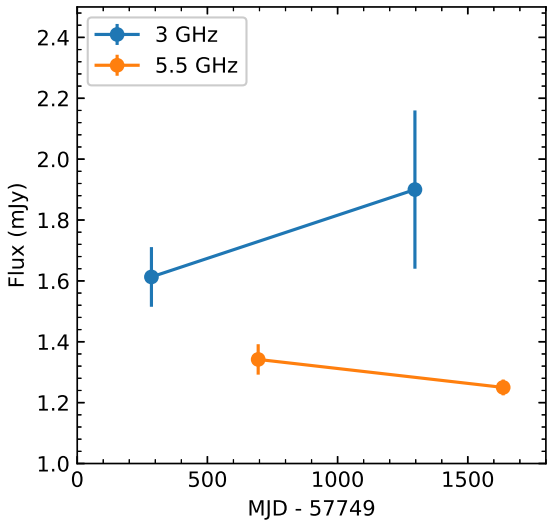

Extended Data Figure 7: **Radio flux of SDSSJ0103+1401 at 3 GHz and 5.5 GHz.**

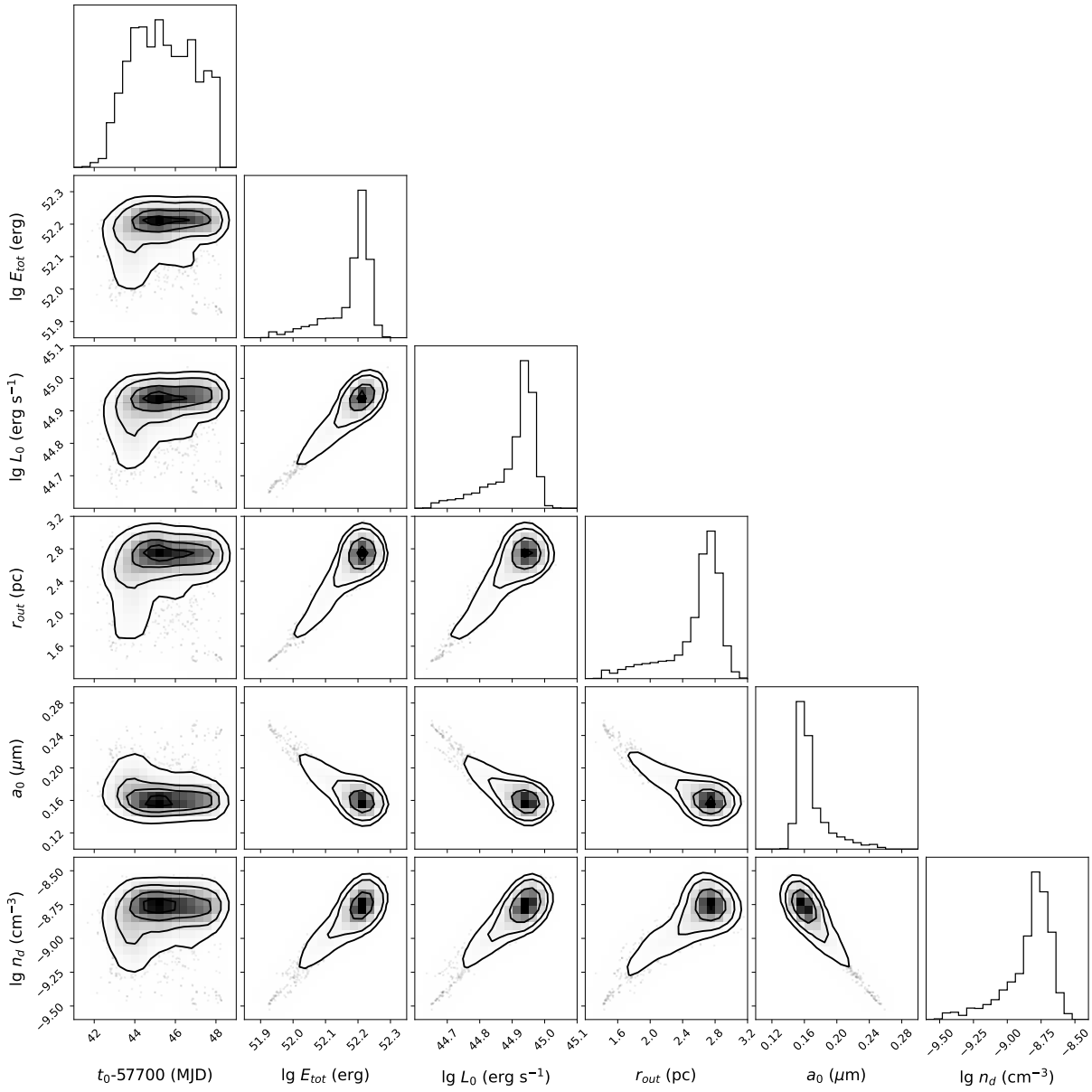

Extended Data Figure 8: **The probability density distribution of the model parameters obtained using MCMC method.**

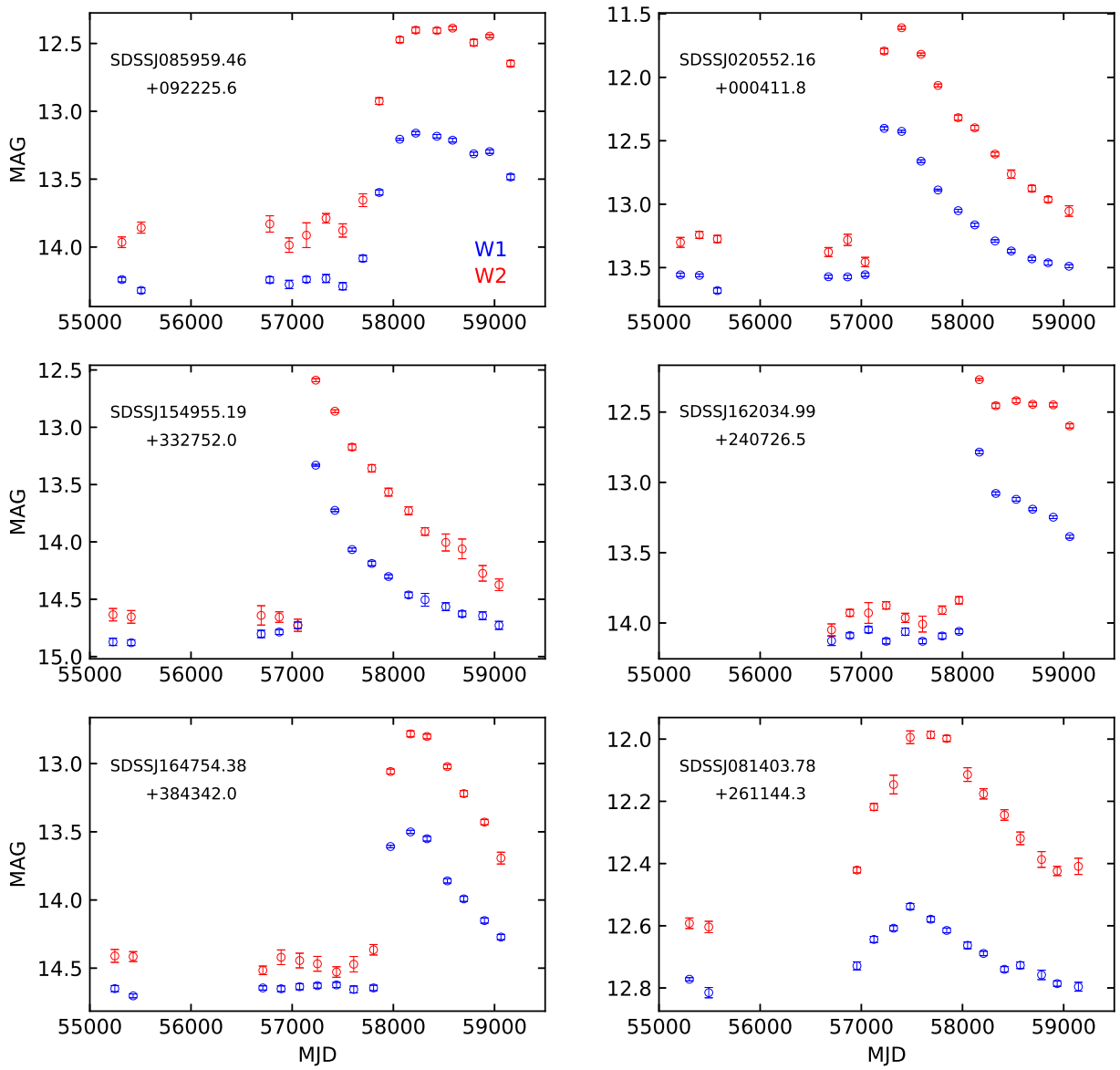

Extended Data Figure 9: **MIR light-curves of some analogs of SDSSJ0103+1401 in MIRONG sample[13].**

Extended Data Table 1: WISE MIR Photometry

Date	MJD	W1	W2	W3	W4
2010 Jan 8	55204.2	11.378(0.011)	11.220(0.013)	...	...
2010 Jul 12	55389.6	11.362(0.011)	11.188(0.010)	7.6(0.019)	4.88(0.029)
2011 Jan 4	55565.7	11.412(0.011)	11.249(0.012)	...	...
2014 Jan 7	56664.6	11.385(0.010)	11.258(0.013)	...	...
2014 Jul 13	56851.7	11.383(0.012)	11.229(0.013)	...	...
2015 Jan 8	57030.1	11.387(0.011)	11.217(0.013)	...	...
2015 Jul 13	57216.5	11.365(0.012)	11.235(0.012)	...	...
2016 Jan 2	57389.5	11.375(0.011)	11.243(0.012)	...	...
2016 Jul 11	57580.6	11.377(0.011)	11.215(0.013)	...	...
2016 Dec 26	57748.7	11.345(0.012)	11.126(0.011)	...	...
2017 Jul 12	57946.0	10.534(0.016)	9.755(0.009)	...	...
2017 Dec 23	58110.4	10.528(0.015)	9.803(0.010)	...	...
2018 Jul 13	58312.0	10.496(0.016)	9.743(0.009)	...	...
2018 Dec 19	58471.6	10.654(0.015)	9.889(0.009)	...	...
2019 Jul 12	58676.0	10.925(0.014)	10.251(0.010)	...	...
2019 Dec 20	58837.5	11.094(0.013)	10.512(0.010)	...	...
2020 Jul 10	59040.6	11.197(0.011)	10.710(0.011)	...	...

Note: We use Vega magnitude. The values in the parentheses are the magnitude errors.

Extended Data Table 2: Optical Photometry

Survey	Photometry	Mjd	Year	V	g
CRTS	Aperture	53636-53773	2005	14.55(0.03)	...
		53976-54128	2006	14.56(0.07)	...
		54276-54495	2007	14.55(0.02)	...
		54741-54849	2008	14.57(0.02)	...
		55072-55242	2009	14.58(0.02)	...
		55365-55587	2010	14.58(0.03)	...
		55823-55958	2011	14.58(0.02)	...
		56150-56329	2012	14.57(0.02)	...
		56532-56598	2013	14.57(0.01)	...
ASAS-SN	Aperture	56193-56676	2013	15.14(0.12)	...
		56797-57043	2014	15.16(0.09)	...
		57169-57409	2015	15.15(0.09)	...
		57531-57774	2016	15.14(0.14)	...
		57897-58121	2017	15.12(0.09)	15.53(0.11)
		58261-58519	2018	15.14(0.08)	15.52(0.12)
		58624-58882	2019	...	15.51(0.11)
		58990-59255	2020	...	15.51(0.11)
		59351-59538	2021	...	15.52(0.15)

Note: Optical data of SDSSJ0103+1401. The median magnitudes in both V and g bands vary less than 0.03 mag indicating SDSSJ0103+1401 has no obvious variability in optical.

Extended Data Table 3: Flare NIR Photometry

Date	MJD	J	H	Ks
2018 Jul 16	58315	18.21(0.70)	15.13(0.03)	13.11(0.04)
2019 Nov 23	58445	18.13(0.74)	15.67(0.05)	13.52(0.05)

Note: The Vega magnitudes of the host subtracted flare in near infrared. The values in the parentheses are the magnitude errors

Extended Data Table 4: Observed properties of SDSSJ0103+1401 host galaxy

SDSS J010320.39+140152.5	
R.A. (SDSS) [J2000.0]	01:03:20.39
Decl. (SDSS) [J2000.0]	+14:01:52.5
Redshift (SDSS)	0.04181
GALEX FUV [μJy]	178 ± 13
GALEX NUV [μJy]	281 ± 11
SDSS u-band [mJy]	0.84 ± 0.01
PS1 g-band [mJy]	2.83 ± 0.04
PS1 r-band [mJy]	4.50 ± 0.14
PS1 i-band [mJy]	6.74 ± 0.07
PS1 z-band [mJy]	7.92 ± 0.15
PS1 y-band [mJy]	9.16 ± 0.17
UKIDSS Y band [mJy]	10.87 ± 0.20
UKIDSS J band [mJy]	12.31 ± 0.13
UKIDSS H band [mJy]	15.62 ± 0.19
UKIDSS K band [mJy]	13.74 ± 0.32
WISE W1-band [mJy]	8.75 ± 0.26
WISE W2-band [mJy]	5.61 ± 0.20
WISE W3-band [mJy]	28.94 ± 0.50
WISE W4-band [mJy]	93.85 ± 2.50
SED fitting parameters with CIGALE	
SFR [$\mathrm{M_\odot\ yr^{-1}}$]	6.3 ± 0.7
Stellar mass [log(M/$\mathrm{M_\odot}$)]	10.53
Reduced χ^2	0.51

Extended Data Table 5: Fitting parameters of dust echo model

t_0 [MJD]	(57742.1, 57748.1)
log($E_{\rm tot}$ [erg])	(51.92, 52.28)
log(L_0 [erg s^{-1}])	(44.65, 45.01)
$r_{\rm in}$ [pc]	$<$0.24
$r_{\rm out}$ [pc]	(1.4, 3.1)
a_0 [μm]	(0.14, 0.25)
log($n_{\rm d}$ [cm^{-3}])	($-$9.48, $-$8.55)

confidence interval with a 99.7% probability.